Driven Alfven waves and electron acceleration: A FAST case study

C. C. Chaston, J. W. Bonnell, L. M. Peticolas, C. W. Carlson, and J. P. McFadden
Space Sciences Laboratory, University of California, Berkeley, California, USA

R. E. Ergun
Laboratory for Atmospheric and Space Physics, University of Colorado, Boulder, Colorado, USA

Received 25 July 2001; accepted 4 October 2001; published 12 June 2002.

[1] Observations of electric and magnetic field oscillations and accelerated electron distributions within an inverted-V region suggest the propagation of an Alfven wave from the outer magnetosphere into the auroral acceleration region. This hypothesis is tested for a case study event by simulating the propagation of an Alfven wave driven by an oscillating potential in the outer magnetosphere. At the spacecraft altitude the waveform and the associated electron distributions and spectra formed due to acceleration in the Alfven wave field are similar to those observed. The results show that more than 50% of the downgoing wave Poynting flux is dissipated through electron acceleration parallel to the geomagnetic field. *INDEX TERMS:* 2407 Ionosphere: Auroral ionosphere (2704); 2716 Magnetospheric Physics: Energetic particles, precipitating; 2752 Magnetospheric Physics: MHD waves and instabilities

1. Introduction

[2] Perhaps the most important aspect of Alfven waves observed in the auroral oval, and more recently in the high latitude magnetosphere [*Wygant et al.*, 2000], is their ability to accelerate electrons to energies and in fluxes sufficient to cause visible aurora [*Chaston et al.,* 2002]. *Hasegawa* [1976] developed the idea that an Alfven wave whose wavelength projected perpendicular to the geomagnetic field ($\mathbf{B}_o$) was of the order of an ion acoustic gyro radius (ρ_i) or less, carries a parallel electric field and can thereby accelerate electrons to form aurora. While this is true at higher altitudes, observations in the auroral oval suggest that electron inertial effects are more important [*Goertz and Boswell*, 1979; *Lysak and Carlson* 1981] and it has been shown that the perpendicular wavelength here is closer to the electron inertial length (λ_e) [*Louarn et al.*, 1994; *Chaston et al.*, 1999] than the ion acoustic gyro-radius. Under such conditions the electrons can no longer be considered massless and so this wave will also carry a parallel field.

[3] The result that the inertial Alfven wave carries a parallel electric field and large amplitude electromagnetic waves with $E/B \geq V_A$ and $k_\perp \lambda_e \geq 1$ are observed from rockets and low altitude spacecraft [*Stasiewicz et al.*, 2000] has motivated a number of studies [*Goertz and Boswell*, 1979; *Kletzing*, 1994; *Hui and Seyler*, 1992; *Thompson and Lysak*, 1996; *Lotko et al.*, 1998; *Clark and Seyler*, 1999; *Kletzing and Hu*, 2001] to examine the ability of such waves to accelerate electrons. In this report we extend the work of *Chaston et al.* [2000] to compare observations of wave-fields and accelerated electron distributions associated with Alfven waves with the predictions of a linear MHD simulation [*Thompson and Lysak*, 1996] which incorporates the important macroscopic features of the plasma above the auroral oval as well as the microscopic effects of electron inertia along auroral geomagnetic fieldlines from 100 km up to 5 Earth radii in altitude.

0094-8276/02/2001GL013842$05.00

2. Observations

[4] Figure 1 shows measurements from the FAST spacecraft in an inverted-V electron event. The first panel shows the electric field ($E_{\perp 1}$) measured perpendicular to the geomagnetic field ($\mathbf{B}_o$) and roughly in the North-South direction. Throughout the interval shown this quantity fluctuates in a nearly periodic fashion with a period from one to two seconds. The perpendicular wave magnetic field ($B_{\perp 2}$), shown in the second panel, has a similar form and provides $E_{\perp 1}/B_{\perp 2} = 1.0 \times 10^4$ km s^{-1}. The field-aligned Poynting flux shown in the third panel indicates wave energy travelling both up (negative) and down (positive) the field line. However the upgoing flux is generally less than that of the downgoing. Assuming a higher altitude source for these waves, suggests that some of the wave energy flux is lost at altitudes below the spacecraft or lost to the ionosphere rather than being reflected back up the fieldline to the magnetosphere.

[5] The electron measurement shown in the last two panels of Figure 1 suggests that some of the missing wave power has been dissipated through electron acceleration. The energy of the inverted-V peak at 5–10 keV in the 4th panel is clearly modulated by the wave field at 11:08:10 and 11:09:00:00 UT at the observed wave frequency where the wave amplitude is largest. In the pitch angle spectra of the last panel the isotropic fluxes representing the inverted-V are pulsed at this frequency. At energies below the inverted-V peak impulsive bursts of field-aligned electrons spaced in time by roughly the wave period are observed. The pitch angle spectra shows that most of these electrons are accelerated down the fieldline (0°) however upward accelerated electrons (180°) within the loss cone are observed around 11:08:10 and 11:09:00:00 UT.

3. Simulation

[6] To model these observations we adopt the approach of *Thompson and Lysak* [1996]. The formalism is that previously described by *Chaston et al.* [2000] and so the model equations will not be repeated here. The Alfven wave is launched by applying a potential variation $\phi_o(t)$ to a dipole field at 5 Earth radii altitude above the auroral oval. The wave scalar ($\phi(z, t)$) and vector potentials ($A(z, t)$) are then determined as a function of time and position along the fieldline. Field fluctuations are assumed to be periodic perpendicular to the dipole field and characterized by a particular wavenumber $k_\perp$ which scales inversely with the flux-tube width. These are given by $E_{\perp 1} = k_\perp \phi(z, t)$ and $B_{\perp 2} = k_\perp A_\parallel(z, t)$ with $E_{\perp 1}(x) = E_{\perp 1}\cos(k_\perp x)$ and $B_{\perp 2}(x) = B_{\perp 2}\cos(k_\perp x)$. The wave frequency is set by the time dependency of $\phi_o(t)$. In this case $\phi_o(t)$ is determined from the observed electric field at the spacecraft altitude under the assumption that the longer period fluctuations are mainly temporal. The amplitude of $\phi_o(t)$ is such that the simulation returns approximately the same wave amplitude at the spacecraft altitude as observed. This is dependent on the density and composition profiles used, n(z) and c(z) (where z is the altitude in km), the

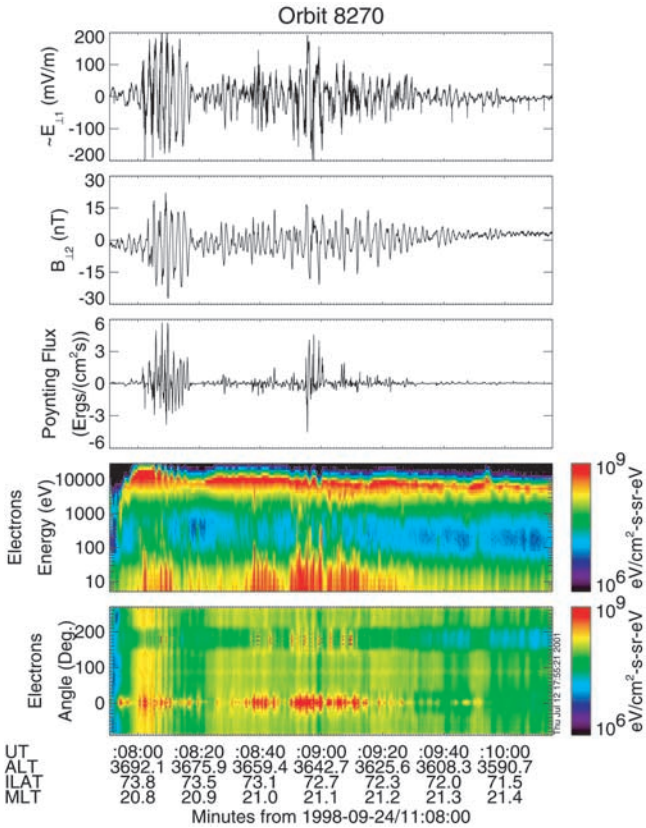

Figure 1. Alfven waves in an inverted-V. The first panel shows the wave electric field measured perpendicular to the geomagnetic field ($\mathbf{B}_o$) and roughly in the north-south direction ($\mathbf{E}_{\perp 1}$). The second panel shows the wave magnetic field measured perpendicular to $\mathbf{B}_o$ and $\mathbf{E}_{\perp 1}$ and roughly in the east-west direction ($\mathbf{B}_{\perp 2}$). The third panel is the field-aligned wave Poynting flux with positive pointing downwards. The fourth and fifth panel are the electron energy and pitch angle spectra with 0° and 180° downwards and upwards along the fieldline respectively.

perpendicular wavenumber, and to a lesser extent is dependent on the height integrated Pedersen conductivity, Σ_p at the ionospheric boundary.

[7] Figure 2 shows the altitude dependent density profiles of O^+ (dashed) and H^+ (dot-dashed) used in the simulation in cm^{-3}. These follow primarily from observations over the range of altitudes covered by FAST and are determined from the electron plasma frequency and other wave emissions [*Strangeway et al.*, 1998] taken over several hundred orbits. The density profile employed has the form $n_O(z) = 400.0z.\exp(-z/175.)$ for O^+ and $n_H = n_M + n_I$ with $n_M = 0.1 + 10.0/(400.0z/Re)^{0.5}$ and $n_I = 100.0z.\exp(-z/280.)$ for H^+, where n_M and n_I are the magnetospheric (plasma sheet) and ionospheric (F-region) contributions respectively. The diamonds represent the average density at that altitude in a bin of 400 km width with the error bars representing the range of values observed. The very low densities reported above 3000 km are those recorded in ion beam regions. The presence of the inverted-V electrons in this case study indicates that such a region exists above the spacecraft and so we have set a density of 1 cm^{-3} at 4000 km to represent this. The solid and dotted lines in this figure show the wave phase speed for the Alfven and inertial Alfven wave respectively. The wavelength in the ionosphere used for the inertial wave dispersion is 5 km.

[8] The electron model consists of two electron components. Plasma sheet electrons continually enter the simulation from the magnetospheric boundary and each is selected randomly from the downgoing half of a 500 eV Maxwellian distribution. There is potential drop included in the model with a total magnitude of 10 keV distributed uniformly over the altitude range from 6000 up to 24,000 km. After a period of time these plasma sheet electrons fill the flux tube down to the ionosphere and the mirrored portion provides a loss cone. Ionospheric electrons with a temperature of 2 eV are distributed along the field line from the ionosphere up to 6000 km in altitude. These are distributed with altitude in a manner representing the density profiles shown in Figure 2 to the extent possible for completing the simulation in a reasonable time. The maximum number of electrons in the simulation at any time is limited to 20,000.

[9] The applied potential model, $\phi_o(t)$, is derived from the observed electric field. For a travelling wave we can approximate the scalar potential at 30,000 km in the absence of wave reflection (or the closure of potential contours above the spacecraft) by mapping $\phi(z, t) = E_{\perp 1}(z, t)/k_\perp(z)$ from the spacecraft altitude. In this approximation, a perpendicular wavelength in the ionosphere of 5 km and, from Figure 1, a wave amplitude of 200 mV/m at 3600 km altitude, requires a scalar potential with amplitude 2200 V at 30,000 km altitude. Using this result, the applied potential at 30,000 km used in the simulation has the form of the observed electric field filtered to remove high frequency fluctuations above 10 Hz with a maximum amplitude of 2500 V. The slightly larger potential has been used to account for losses in downgoing Poynting flux due to reflection.

[10] Selection of perpendicular wavelengths in the ionosphere between 2 km and 10 km do not appreciably alter the results since the maximum energy that electrons reach in the wave does not alter greatly. Outside this range however, the energy decreases particularly at wavelengths less than 2 km.

4. Simulation Results and Observations

[11] Figure 3 shows a 'zoomed-in' portion of Figure 1 where burst data was available and results obtained from the simulation described above displayed in the same format obtained from a virtual FAST spacecraft flying through the simulation at 3600 km altitude. The plotted dynamic range of the observed electron fluxes has been limited to one order of magnitude to provide a range similar to that obtainable by the simulation. This results in a very narrow inverted-V peak in energy. Given that the only observational inputs to the model is the observed electric field mapped to 30000 km and the statistical Alfven speed profile, the similarity between the observations and simulation is reasonable. The similarity between the observed and predicted waveforms in $E_{\perp 1}$ and $B_{\perp 2}$ verifies that indeed these fluctuations are Alfvenic in nature.

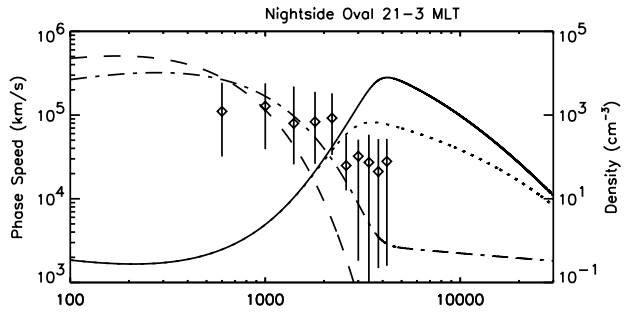

Figure 2. Density and phase speed profiles. The diamonds are statistically determined average values for density from FAST data in the nightside oval from 21-03 MLT. The error bars are the range of density values observed at that altitude. The dashed and the dot dashed lines are the O^+ and H^+ density in the model respectively. The solid and dotted lines are the Alfven and inertial Alfven phase speeds respectively for a perpendicular wavelength ($\lambda_\perp$) in the ionosphere of 5 km.

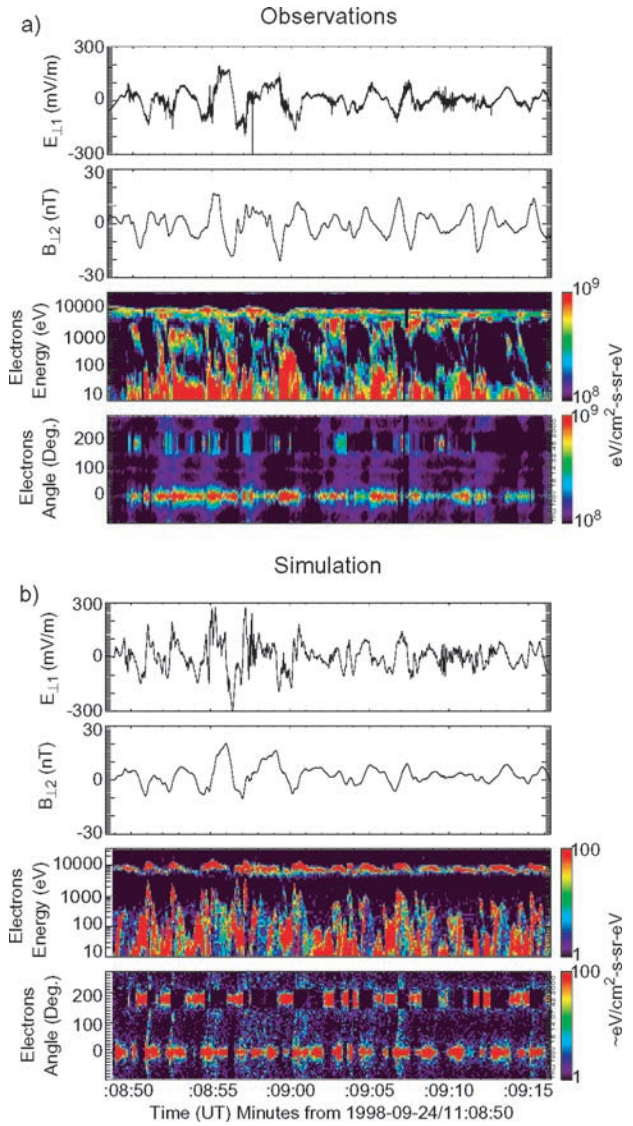

Figure 3. Real (a) and simulated (b) FAST observations. (a) shows a segment of high resolution FAST data from Figure 1 while (b) is the simulated result obtained by a virtual FAST spacecraft in the simulation at the same altitude and for the same time interval as shown in (a).

There is however a phase shift difference. In the observations the magnetic field leads the electric field by ~45° while in the simulation the reverse is true. The phase difference observed is altitude dependent and related to the parallel wavelength and the altitude where wave reflection occurs. For a purely travelling wave $E_{\perp 1}$ and $B_{\perp 2}$ should be in phase or 180° out of phase while for a standing wave these field quantities will be 90° out of phase. Clearly the observations and simulation wavefields presented in Figure 3 are a mixture of the incident and reflected wavefields leading to an intermediate phase difference at the altitude of observation as discussed by *Lysak* [1991].

[12] The electron spectra while not replicated in detail is qualitatively similar to that observed. The wave field can be seen to modulate the energy flux of the inverted-V electrons and provide suprathermal electron bursts at energies below this peak. As shown by the pitch angle spectra these field-aligned bursts are both up (0°) and downgoing (180°) along the field line. The most energetic of the field-aligned electrons are accelerated from the base of the potential drop at 6000 km where the parallel electric field and wave phase speed is largest. The lower energy electrons have source altitudes in the vicinity of the spacecraft itself and hence there is almost no time dispersion in the simulation. The upgoing fluxes are relatively larger in the simulation than observed presumably due to a weaker mass density gradient below the spacecraft in the simulation than in the real case. This allows the simulated wave to carry a larger parallel electric field at lower altitudes than the observations suggest, resulting in greater lower altitude acceleration both up and down the fieldline. This may also account for the somewhat more dispersive nature of the observed electron bursts relative to those simulated since it implies a higher source altitude for the most energetic electrons observed.

[13] Electron energies for the simulated field-aligned bursts are comparable to those observed except in the most energetic cases where energies extend up to 10 keV (see for example of 11:09:02.5 UT). Given the form of these observations in the energy spectra it seems likely some of this energy is obtained from the potential drop where ionospheric electrons have penetrated through the sheath surrounding the potential drop from the sides [*Lotko*, 1986]. An allowance for such a process has not been included in the simulation.

[14] Figure 4 shows snapshots of the observed and simulated pitch angle distributions at a time when field-aligned counterstreaming electrons are observed. The electron energy flux in the downgoing beam (0°) in both observations and simulation is strongly field-aligned and well within the source cone of electrons which reach the ionosphere to form aurora. The distribution is relatively flat in the parallel direction with energy from 100 eV to 2 keV resulting from parallel wave heating of the ionospheric electron component. This is a feature observed in electron distributions at altitudes where Alfven-wave electron acceleration occurs. At lower altitudes (below the peak in the Alfven speed shown in Figure 2), where the wave slows down and the resonant electrons move ahead of the wave, time of flight dispersion leads to

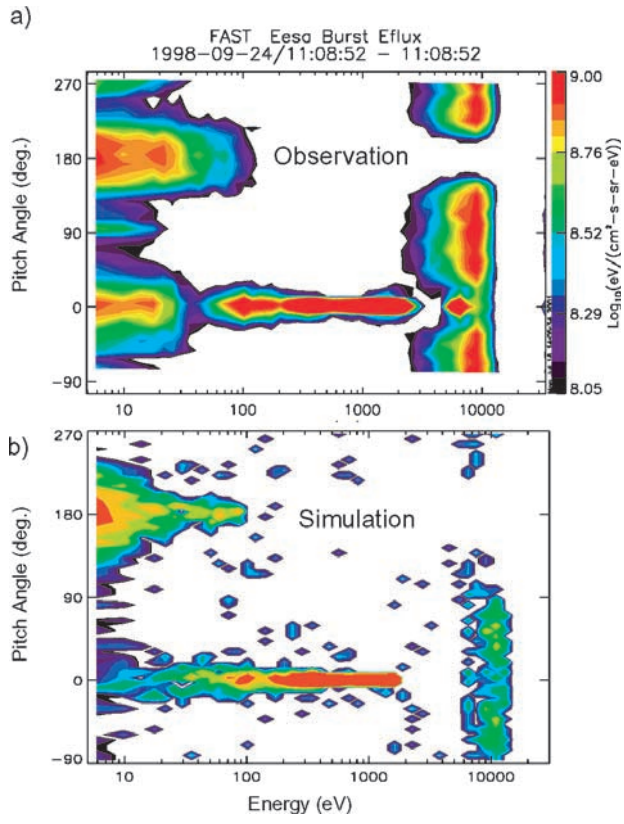

Figure 4. Electron pitch angle distributions from a slice through the observed (a) and simulated (b) electron data shown in Figure 3.

a more peaked distribution. The upgoing electrons at this altitude have energies less than 100 eV. These particles are trapped in the wave field during the reflection process below the spacecraft and carried back up the fieldline until they are reflected back downwards by the DC parallel field. At the base of the potential drop these electrons have energies of up to a few keV and have distributions very similar to the downward accelerated electrons shown in Figure 4.

[15] For the test particle results to be meaningful the energy flux in the accelerated electron distributions must be less than or equal to the wave Poynting flux at the source when both quantities are mapped to the same altitude. An estimate of the particle energy flux incident on the ionosphere assuming that all the accelerated electrons are within the source cone is given by $S_p = \frac{1}{T}\int_{100}^{H} n(z)\overline{E}(z)\sqrt{B_0(100)/B_0(z)}dz$ where T is the wave transit time through the altitude range where the acceleration occurs and E(z) is the average energy that a particle from altitude z receives from the wave. This integration is performed numerically over the range from 100 km altitude up to the top of the simulation box (H) at 30,000 km. For a 1.7s transit time we obtain a maximum integrated energy flux of 10.6 ergs cm^{-2} s^{-1} over the length of the simulation. The corresponding applied wave Poynting flux mapped from 30,000 km to 100 km is 13.7 ergs cm^{-2} s^{-1}. It can be seen that in this case most of the wave energy is dissipated through electron acceleration. If instead we map the simulated Poynting flux from 3600 km to the ionosphere at 100 km we obtain a value of 9.0 ergs cm^{-2} s^{-1} indicating that a significant portion of the wave energy flux has already been reflected above this altitude. Observations show a similar relationship between wave Poynting flux and electron energy flux. Mapping the observed electron energy flux at 3600 km altitude to the ionosphere yields a maximum of 5.1 ergs cm^{-2} s^{-1} for electrons at energies below the inverted-V peak shown in Figure 1. The Poynting flux from the same figure shows a maximum of 6.0 ergs cm^{-2} s^{-1}. Due to partial wave reflection and dissipation at altitudes above the point of observation it can be expected that the Poynting flux for the same wave, if observed at 30,000 km, and mapped from this altitude would be larger than this value.

5. Conclusion

[16] A 1-D MHD model for Alfven wave propagation in the auroral oval has been used successfully to model field and electron observations from a FAST case study. By using the observed electric wave field to determine the form of the applied potential or magnetospheric driver the observed waveforms at the spacecraft altitude have been reproduced. Landau resonance and quasi-static DC potential accleration of electrons in the parallel electric wave field of the inertial Alfven wave provides electron energies sufficient in this case to account for the all but the very largest observed peak electron energies. The wave acceleration process also heats the ionospheric electron distribution by keV's in the direction parallel to the geomagnetic field and produces field-aligned electron bursts distributed in pitch angle qualitatively similar to observations. More than 50% of the downgoing wave Poynting flux is converted to downgoing electron energy flux in this process.

[17] **Acknowledgments.** This work benefited from discussions with R. L. Lysak and W. Lotko and was supported by NASA grant NAG5-3596 and the Physics Department at the Chinese University of Hong Kong.

References

Chaston, C. C., C. W. Carlson, W. J. Peria, R. E. Ergun, and J. P. McFadden, FAST observations of inertial Alfven waves in the dayside aurora, *Geophys. Res. Lett.*, *26*, 647, 1999.

Chaston, C. C., C. W. Carlson, R. E. Ergun, and J. P. McFadden, Alfven waves, density cavities and electron acceleration observed from the FAST spacecraft, *Physica Scripta*, *T84,* 2000.

Chaston, C. C., L. M. Peticolas, J. W. Bonnell, C. W. Carlson, R. E. Ergun, and J. P. McFadden, The width and brightness of auroral arcs driven by inertial Alfven waves', *J. Geophys. Res.*, in press, 2002.

Clark, A. E., and C. E. Seyler, Electron beam formation by small-scale oblique inertial Alfven waves, *J. Geophys. Res.*, *104*, 17,233, 1999.

Hasegawa, A., Particle acceleration by MHD surface wave and formation of aurora, *J. Geophys. Res.*, *81*, 5083, 1976.

Hui, C.-H., and C. E. Seyler, Electron accleration by Alfven waves in the magnetosphere, *J. Geophys. Res.*, *97*, 3953, 1992.

Goertz, C. K., and R. W. Boswell, Magnetosphere-ionosphere coupling, *J. Geophys. Res.*, *84*, 7239, 1979.

Kletzing, C. A., Electron acceleration by kinetic Alfven waves, *J. Geophys. Res.*, *99*, 11,095, 1994.

Kletzing, C. A., and S. Hu, Alfven wave generated electron time dispersion, *Geophys. Res. Lett.*, *28*, 693, 2001.

Lotko, W., A. Streltsov, and C. W. Carlson, Discrete auroral arcs, electrostatic shock and suprathermal electrons powered by dispersive anomalous resistive fieldline resonance, *Geophys. Res. Lett.*, *25*, 4449, 1998.

Lotko, W., Diffusive acceleration of auroral primaries, *J. Geophys. Res.*, *91*, 191, 1986.

Louarn, P., J.-E. Wahlund, T. Chust, H. de Feraudy, A. Roux, B. Holback, P. O. Dovner, A. I. Eriksson, and G. Holmgren, Observations of kinetic Alfven waves by the Freja spacecraft, *Geophys. Res. Lett.*, *21*, 1847, 1994.

Lysak, R. L., and C. W. Carlson, Effect of microscopic turbulence on magnetosphere-ionosphere coupling, *Geophys. Res. Lett.*, *8*, 269, 1981.

Lysak, R. L., Feedback instability of the ionospheric resonant cavity, *J. Geophys. Res.*, *96*, 1553, 1991.

Stasiewicz, K., et al., Small Scale Alfvenic Structure in the Aurora, *Sp. Sci. Rev.*, *92*, 423, 2000.

Strangeway, R. J., et al., FAST observations of VLF waves in the auroral zone: Evidence of very low plasma densities, *Geophys. Res. Lett.*, *25*, 2065, 1998.

Thompson, B. J., and R. L. Lysak, Electron acceleration by inertial Alfven waves, *J. Geophys. Res.*, *101*, 5359, 1996.

Wygant, et al., Polar spacecraft comparisons of intense electric fields and Poynting flux near and within the plasma sheet-tail lobe boundary to UVI images: An energy source for the aurora, *J. Geophys. Res.*, *105*, 18,675, 2000.

C. C. Chaston, J. W. Bonnell, L. M. Peticolas, C. W. Carlson, and J. P. McFadden, Space Sciences Laboratory, University of California, Berkeley, CA 94720, USA. (ccc@ssl.berkeley.edu)

R. E. Ergun, Laboratory for Atmospheric and Space Physics, Campus Box 590, Boulder, CO 80309, USA.